

STUDY ON CONSTRAINT EFFECT AND CREEP CRACK INITIATION OF PLATE CONTAINING ELLIPTICAL EMBEDDED CRACKS

DONGQUAN WU, ZIXIANG LIU, YUPENG LI, DINGHE LI

Sino-European Institute of Aviation Engineering, Civil Aviation University of China, Tianjin, China
corresponding author Dongquan Wu, e-mail: dquwu@cauc.edu.cn

ZHIQIANG ZHANG

Aviation Engineering Institute, Civil Aviation University of China, Tianjin, China

In this study, a plate structure containing elliptical embedded cracks loaded under high temperature is studied. The constraint effect and creep crack initiation of the plate containing embedded cracks are discussed by using the finite element method based on the creep ductility exhaustion model. It is indicated that the highest constraint level or the load-independent parameter Q^* is observed at the endpoint of the ellipse major axis of an elliptical embedded crack, and the constraint levels increase with crack length or depth, which represents a worse condition for the structure, such as higher stress concentration and greater danger of failure for a larger crack depth ratio a/t or crack length ratio a/c . Moreover, under the creep condition, the embedded crack with a larger a/t , a/c or loadings is accompanied with a higher crack driving force, which can accelerate creep damage, creep cracking initiation (CCI) and shorten the creep crack initiation (CCI) time. Additionally, an empirical prediction equation and engineering approach to the constraint parameter and the CCI time for elliptical embedded cracks are proposed, and the engineering approach to the CCI time is validated.

Keywords: elliptical embedded crack, creep crack initiation time, creep ductility exhaustion model, constraint parameter

Highlights:

- (1) The constraint effect and creep crack initiation of a plate containing embedded cracks are discussed by using the finite element method based on the creep ductility exhaustion model.
- (2) The highest constraint level is observed at the endpoint of the ellipse major axis of the elliptical embedded crack, and the constraint levels increase with crack length or depth, while the creep crack initiation time exhibits a contrary trend.
- (3) An empirical prediction equation and engineering approach of the constraint parameter and creep crack initiation (CCI) time is proposed, and the engineering approach is validated.

1. Introduction

In recent years, the modern industrial core equipment (such as aeroengines, ultra supercritical generator sets, nuclear power generator sets, etc.) with higher energy conversion efficiency and lower pollution emission rate is vigorously developed in order to conserve energy, reduce pollution emission and protect the environment. To continuously improve energy conversion efficiency, all of the modern industrial core equipment is designed for operating under higher temperature, which will lead to increasingly harsh in-service conditions of the hot side components (Chen *et al.*, 2004).

The integrity assessment of high temperature in-service components such as power plants and aeroengines is generally inseparable from reliable prediction of creep properties and creep life. For

steam pipes, aeroengines and other structures operating in elevated temperature environment, initial defects such as cracks may occur during their processing (such as welding) or after a long time service, which will have a significant influence on components safety in the subsequent service. Creep crack initiation and creep crack propagation are important failure mechanisms for high temperature structures containing cracks, which usually leads to failure or fracture of these structures before their allowable service life (Yamamoto *et al.*, 2010; Murakami *et al.*, 1988; Zhao *et al.*, 2012). Specially, the creep crack initiation time is the critical and longest period of the whole creep life for high-temperature components. To ensure safety and reliability of high-temperature service structures, taking investigation on the creep crack initiation time is extremely important (Davies *et al.*, 2007). The creep crack initiation time is generally defined as the time when initial microcracks (or micro cavities) in the structure or material begin to connect and form the main crack under the creep condition. The generation, growth and connection processes of creep micro cavities and creep microcracks are referred as to creep damage. A large number of theories and experiments have proved that the creep cracks initiation and creep cracks propagation are the main failure forms of structures (Holdsworth, 1992).

Among the current evaluation methods of creep cracks initiation time, the finite element simulation method or an analytical prediction model based on the continuous damage approach have special advantages. The creep damage model mainly includes two types: one is the damage constitutive model based on the stress variable (Hosseini *et al.*, 2013), and the other is the damage constitutive model based on the strain variable (Yatomi *et al.*, 2004). The former typical type of model are the Kachanov Rabotnov (K-R) model (Rabotnov *et al.*, 1970) and Liu Murakami (L-M) model (Liu and Murakami, 1998). For example, Mao *et al.* (2004), You *et al.* (2004) and Chen *et al.* (2014) used K-R and L-M models to analyze creep damage and creep life prediction of materials and structures by the finite element method, respectively, which allowed obtaining satisfactory research results. In the latter type of model, the classic creep ductility exhaustion model proposed by Cocks and Ashby (1980) adopts one single parameter as the damage variable and involves few material parameters, so the model is simple and convenient to be applied in engineering fields. The basic principle of the damage model is that when the cumulative creep strain of a micro-element on the material reaches the creep fracture strain (or creep ductility), it is considered that the damage of this micro-element reaches the critical value and fails. Riedel and Rice (1980) were first to propose a definition of the creep crack initiation time under steady state creep by using the critical equivalent strain produced at a specified distance, that is, when all the microelements at a given distance fail, it is considered that the creep crack initiation time has been reached. Davies (2006) established a prediction method of creep crack initiation time under different stress states based on the creep ductility exhaustion model, Norton's constitutive law and crack tip fracture parameters. Among these theoretical models, the accuracy of the model under transient creep condition was the best.

Wu *et al.* (2020) then applied the C^*-Q^* two parameter method of the crack tip stress field considering constraint parameters into the damage model, and proposed a two parameter prediction approach of the creep crack initiation time. Because of considering the influence of the constraint effect, this approach could be well applied to predict the creep crack initiation time for different structures containing cracks. However, this prediction model is only applied to predict the creep crack initiation time for some standard laboratory specimens or specific pipeline structures containing surface cracks, while its applicability to other structures containing other kinds of cracks needs further study.

The constraint effect refers to the influence of such factors as size and shape of a specimen, crack size and loading configuration on the analytical stress field or strain field at the crack tip, which will further affect the predicting accuracy of creep crack damage or creep crack life. The results of theoretical and experimental studies showed that the geometrical shape, size and loading configurations could all have different effects on the process of creep crack initiation,

crack propagation and creep failure. For this reason, the HRR field based on a single parameter cannot accurately characterize the stress field at the crack tip for different cracked structures (Shih and German, 1981). In order to establish a theoretical modification to accurately describe the stress field at the crack tip, researchers have focused on various two-parameter models of the stress field considering the constraint effect which is suitable for elasto-plastic or creep conditions. Budden and Ainsworth (1999) proposed an in-plane constraint parameter Q suitable for high temperature conditions, and the C^* - Q two-parameter model describing the stress field at the creep crack tip for a high-temperature cracked structure. Xu *et al.* (2016) proposed a load-independent constraint parameter Q^* , and the C^* - Q^* two-parameter creep stress field applicable to structures containing surface cracks at elevated temperature.

At present, the creep crack growth behavior is mainly focused on two-dimensional through-wall specimen cracks and surface cracks, but the research on embedded cracks is relatively rare, while the embedded cracks are difficult to detect before failure and they are especially dangerous crack types. Therefore, it is of great significance to investigate the distribution of creep stress, creep damage, constraint effect and creep life for structures containing embedded cracks. In this paper, based on a typical creep ductility exhaustion model, the finite element method is used to simulate the creep damage of the plate structure containing embedded cracks. The distribution law of the load-independent constraint parameter Q^* along the crack front and the influence of crack size on the creep crack initiation time are analyzed. Finally, the engineering prediction methods of the constraint parameter Q^* and creep crack initiation time are established by fitting a mathematical relationship between the constraint parameter Q^* and creep crack initiation time as well as geometrical sizes of embedded cracks (i.e. crack length ratio a/c and crack depth ratio a/t). The study provides a technical support and theoretical basis for creep crack life assessment of high temperature service components containing embedded cracks.

2. Methodology

2.1. Creep ductility exhaustion approach

In this study, the strain-based creep ductility exhaustion approach proposed by Cocks and Ashby (1980) is used to evaluate creep damage ahead of the crack tip. The typical form of the creep damage rate can be described as follows

$$\dot{\omega} = \frac{\dot{\varepsilon}_c}{\varepsilon_f^*} \quad (2.1)$$

where $\dot{\varepsilon}_c$ and ε_f^* are the creep strain rate and multiaxial creep ductility, respectively. For the creep strain rate, Norton model is adopted

$$\dot{\varepsilon}_c = A\sigma^n \quad (2.2)$$

The multiaxial creep ductility can be obtained by multiplying the uniaxial creep ductility and multiaxial creep ductility factor (*MCDF*)

$$\varepsilon_f^* = MCDF\varepsilon_f \quad (2.3)$$

where the uniaxial creep ductility is generally taken as a constant, and multiaxial creep ductility factor (*MCDF*) can be effectively assessed by the Wen-Tu model (Wen and Tu, 2014)

$$MCDF = \frac{\exp\left(\frac{2}{3} \frac{n-0.5}{n+0.5}\right)}{\exp\left(2 \frac{n-0.5}{n+0.5} h\right)} \quad (2.4)$$

where h is the stress triaxiality which can be calculated by

$$h = \frac{\sigma_m}{\bar{\sigma}} \quad (2.5)$$

where σ_m is hydrostatic stress and $\bar{\sigma}$ is equivalent stress.

The above creep ductility exhaustion model can be compiled into Abaqus software as a Creep subroutine using Fortran language. When submitting the finite element simulation, the subroutine is loaded into the finite element model through the relevant interface for calculation, so as to realize the simulation of creep damage (Wu *et al.*, 2020). In this study, the creep crack initiation (CCI) time is defined as the time when the damage value ω at 0.05 mm ahead of the crack tip reaches unity (Murakami *et al.*, 1988). These CCI data are extracted from the output of finite element simulation results.

In this study, the material properties of P92 heat-resistant steel under 650°C in-service temperature are used in the finite element model, and P92 steel is widely used in ultra supercritical units. The details of the mechanical properties of P92 steel at 650°C are summarized in Table 1, where mainly elasto-plastic and creep parameters are given (Wu *et al.*, 2020). The uniaxial creep ductility is taken as a constant of 20%, as used in reference (Wu *et al.*, 2020).

Table 1. Material properties of P92 steel at 650°C

Young modulus E [MPa]	Yielding stress σ_0 [MPa]	Creep coefficient A [MPa $^{-n}$ h $^{-1}$]	Creep exponent n	Uniaxial creep ductility ε_f [%]
125000	180	$2.6353 \cdot 10^{-16}$	5.23	20

2.2. Constraint parameter

Budden and Ainsworth (1999) proposed an in-plane constraint parameter Q suitable for high temperature conditions, as well as a C^* - Q two-parameter model describing the stress field

$$\sigma_{ij} = \sigma_0 \left(\frac{C^*}{\dot{\varepsilon}_0 \sigma_0 I_n r} \right)^{\frac{1}{n+1}} \tilde{\sigma}_{ij}(\theta; n) + Q \sigma_0 \delta_{ij} \quad (2.6)$$

where C^* integral represents the fracture parameter under a steady state creep condition at the crack front, which is extracted from the finite element simulation results. $\dot{\varepsilon}_0$ and σ_0 are the normalized creep strain rate and yield stress, respectively. r is the distance away from the crack tip, and θ is the angle between the crack direction and research position. $\tilde{\sigma}_{ij}(\theta; n)$ is a dimensionless function of n and θ , and I_n is a parameter related to the creep stress-hardening exponent n . δ_{ij} is the Kronecker delta function ($\delta_{ij} = 1$ for $i = j$ and $\delta_{ij} = 0$ for $i \neq j$). The constraint parameter Q is always determined by the difference of crack opening stress between the specimen structure and the analytical creep stress field

$$Q = \frac{\sigma_{22}^{FEM}(r, 0) - \sigma_{22}(r, 0)}{\sigma_0} \quad (2.7)$$

where $\sigma_{22}^{FEM}(r, 0)$ is the crack opening stress obtained from finite element simulation, and $\sigma_{22}(r, 0)$ is the theoretical creep stress field calculated by

$$\sigma_{ij} = \sigma_0 \left(\frac{C^*}{\dot{\varepsilon}_0 \sigma_0 I_n r} \right)^{\frac{1}{n+1}} \tilde{\sigma}_{ij}(\theta; n) \quad (2.8)$$

Xu *et al.* (2016) then proposed a load-independent constraint parameter Q^* and a C^* - Q^* two-parameter creep stress field

$$Q^* = \left(\frac{C^*}{\dot{\epsilon}_0 \sigma_0 I_n L} \right)^{\frac{-1}{n+1}} Q = \left(\frac{C^*}{\dot{\epsilon}_0 \sigma_0 I_n L} \right)^{\frac{-1}{n+1}} \frac{\sigma_{22}^{FEM}(r, 0) - \sigma_{22}(r, 0)}{\sigma_0} \tag{2.9}$$

$$\frac{\sigma_{ij}}{\sigma_0} = \left(\frac{C^*}{\dot{\epsilon}_0 L I_n \sigma_0} \right)^{\frac{1}{n+1}} \left[\left(\frac{L}{r} \right)^{\frac{1}{n+1}} \tilde{\sigma}_{ij}(\theta; n) + Q_{RRss}^* \delta_{ij} \right]$$

where L is the normalized length generally set as 1 mm (Xu *et al.*, 2016).

In this study, the mechanical parameters of P92 steel at 650°C are used, and more related high temperature properties are summarized in Table 2.

Table 2. Mechanical parameters of P92 steel at 650°C

Normalized creep strain rate $\dot{\epsilon}_0$ [1]	Constant parameter I_n	Dimensionless function $\tilde{\sigma}_{ij}(\theta; n)$	Normalized length L [mm]
$8.8183 \cdot 10^{-5}$	4.99	0.48	1

2.3. Finite element method

A flat plate structure containing embedded cracks is used as the research objective in this study. In general, non-penetration cracks are usually simplified as elliptical in engineering applications, as shown in Fig. 1. According to symmetry of the plate structure, only one eighth of the plate structure is taken in the finite element model for simulation. The three-dimensional finite element model is shown in Fig. 2. The length, width and thickness of the model are 50 mm, 15 mm and 2.5 mm ($= t/2$), respectively. a is a half of the crack depth of the elliptical crack along the thickness direction of the plate, and c is a half of the crack length along the width direction of the plate. In order to conveniently characterize the distribution of constraint parameters at the front of elliptical crack, the angle between the center of the ellipse and any point on the elliptical crack front is denoted as Φ . For convenience of describing the position of the research point, the center of the elliptical crack is taken as the origin, of which $2\Phi/\pi = 0$ represents the rightmost endpoint of the elliptical crack, where there is a intersection of the elliptical crack and the center line of the plate. $2\Phi/\pi = 1$ represents the uppermost endpoint of the elliptical crack, which is the shallowest position of the elliptical crack in the structural thickness direction. Note that in this study, the center of the elliptical crack is just set in the center position of the plate structure. According to the symmetry, symmetrical constraints are set in the three symmetry planes, respectively, and the uniformly distributed load along the length direction is set in the section where it is far from the crack end to realize the loading process, as shown in Fig. 2.

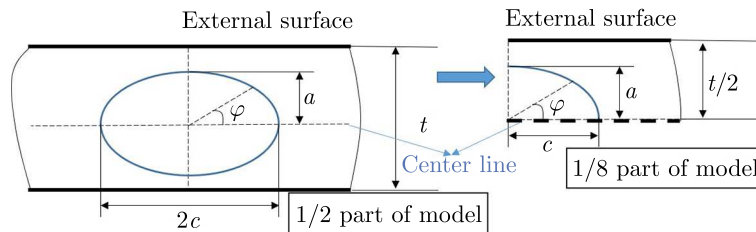


Fig. 1. Geometrical illustrations of the plate structure containing an embedded crack

Figure 3 shows mesh distribution of the three-dimensional finite element model of the plate structure containing the elliptical embedded crack. The area around the crack front adopts a local refined mesh with the minimum mesh size of 0.01 mm. This is to ensure that it is easy to

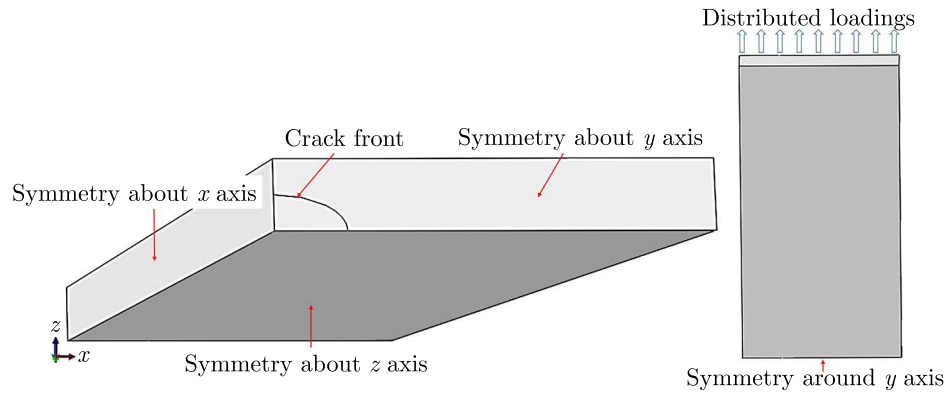


Fig. 2. 1/8 finite element model of the plate structure containing an embedded crack

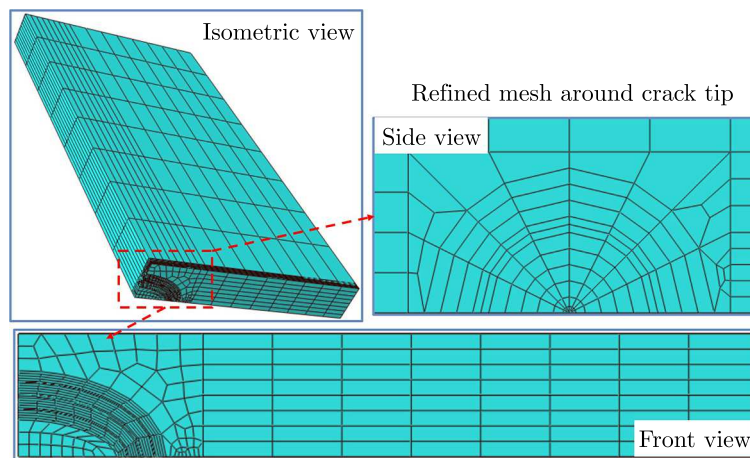


Fig. 3. Mesh of the finite element model of the plate structure containing an embedded crack

obtain the critical distance in the FE model (Wu *et al.*, 2020) for extracting the creep initiation time. The mesh size at other locations is about 0.1 mm-2 mm. The element type of the eight node reduced integral (C3D8R) element is adopted for the model, which exhibits good mechanical calculation accuracy for three-dimensional solid models. The total number of elements of all finite element models with different embedded crack sizes is similar (Wu *et al.*, 2020), because the finite element models use the same mesh refinement size near the crack tip. The total number of elements is about 1800-2100, and the total number of nodes is about 2500-2700.

3. Results and discussion

3.1. Results and analysis of constraint parameters

In order to avoid the influence of the plastic zone ($r < 0.1$ mm) around the crack tip and to ensure that the value of r is within the effective zone of stress concentration at the crack tip, the constraint parameter Q^* is defined by referring to the fixed distance $r = 0.2$ mm (Wu *et al.*, 2020; Xu *et al.*, 2016), and then a large Q^* value can be obtained to ensure the accuracy of calculation, as shown in Fig. 4.

Figure 5 compares the distribution of the constraint parameter Q^* varied with the angle position ($0 \leq 2\Phi/\pi \leq 1$) ahead of the elliptical crack front with the crack depth ratio $a/t = 0.25$ and the crack length ratio $a/c = 0.5, 0.7, 1.0, 1.2, 1.5$. It can be seen from the figure that at the position of $2\Phi/\pi = 1$, i.e the intersection point of the crack front and the center line of the plate

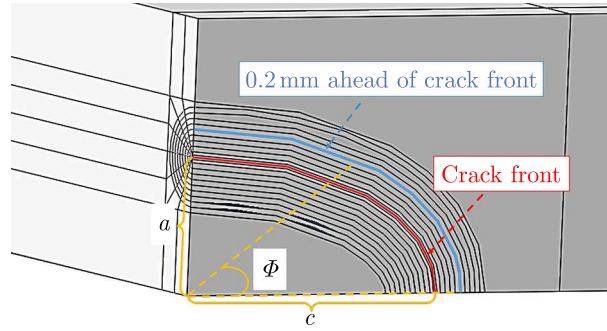


Fig. 4. Research position of the constraint parameter

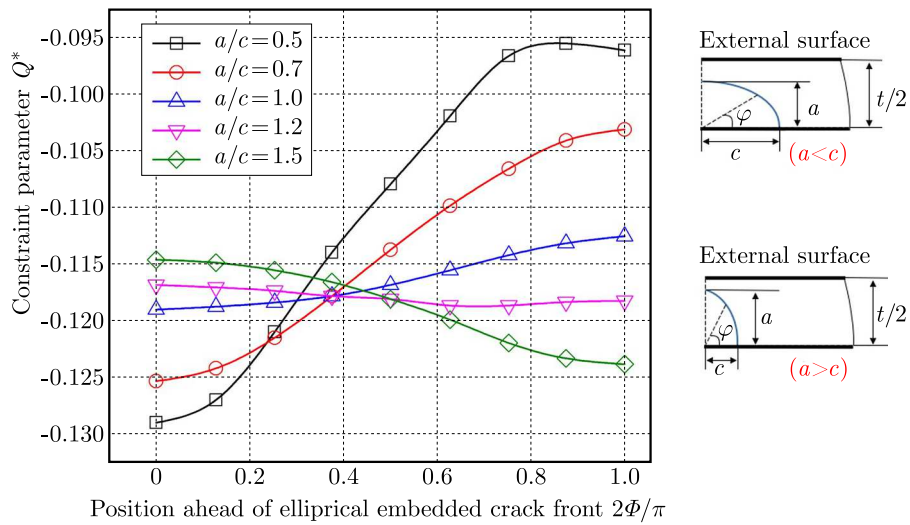


Fig. 5. Distributions of the constraint parameter ahead of the crack front for embedded cracks with various a/c and $a/t = 0.25$

or the rightmost endpoint of the elliptical crack, the constraint parameter Q^* decreases with an increase of the crack length ratio a/c , while at the position of $2\Phi/\pi = 0$, i.e the shallowest position of the crack in the thickness direction of the plate or the uppermost endpoint of the elliptical crack, the constraint parameter Q^* increases with the crack length ratio a/c .

In addition, for an elliptical embedded crack with the same crack depth ratio a/t , the distribution of the maximum constraint parameter Q^* is affected by the crack length ratio a/c . For the elliptical embedded crack with the transverse length c larger than the longitudinal length a (i.e. $a/c \leq 1.0$, refers to the three curves with $a/c = 0.5, 0.7$ and 1.0 in Fig. 5), the long axis of the elliptical crack front is distributed laterally (the shape of the elliptical crack is shown at the top right in Fig. 5), and the maximum value of the constraint parameter Q^* is distributed at the position of $2\Phi/\pi = 1$ (i.e. the uppermost endpoint of the elliptical crack front), and the constraint parameter Q^* at the position $2\Phi/\pi = 0$ (i.e. the rightmost endpoint of the elliptical crack front) is the minimum. For the elliptical embedded crack with the transverse length c less than the longitudinal length a (i.e. $a/c \geq 1.0$, refers to the three curves with $a/c = 1.2$ and 1.5 at the bottom right in Fig. 5), the long axis of the elliptical crack front is longitudinally distributed (the shape of the elliptical crack is shown at the top right in Fig. 5), and the maximum value of the constraint parameter Q^* is distributed at the position of $2\Phi/\pi = 0$ (i.e. the rightmost endpoint of the elliptical crack front), and the constraint parameter Q^* at the position $2\Phi/\pi = 1$ (i.e. the uppermost endpoint of the elliptical crack front) is the minimum.

Therefore, the maximum constraint level around the crack front always appears near the endpoint of the actual major axis of the elliptical crack, while the minimum constraint level

always appears at the endpoint of the actual minor axis of the elliptical crack, no matter whether the major axis is distributed laterally or longitudinally. This phenomenon is caused by the maximum crack propagation under tension at the end of the long axis of the crack. Briefly, with an increase of the crack length ratio a/c , the constraint parameter at the end of the long axis of the elliptical crack increases continuously, which means that the stress concentration here is more severe, the material here is more endangered, and creep crack initiation occurs first. Such conclusions are similar to those of other researchers on the distribution of constraint parameters of semi elliptical surface cracks (Wu *et al.*, 2020; Xu *et al.*, 2016).

Taking the relevant data at the location where creep initiation is most likely to occur, the relationship between the constraint parameter Q^* and crack length a/c can be established with a fixed crack depth $a/t = 0.25$. The specific formula obtained after fitting is as follows

$$Q^* = \alpha + (1 - \alpha) \left\{ 1 - \exp \left[-\beta_1 \frac{a}{c} - \beta_2 \left(\frac{a}{c} \right)^2 - \beta_3 \left(\frac{a}{c} \right)^3 \right] \right\} \quad (3.1)$$

where α , β_1 , β_2 and β_3 are fitting coefficients respectively, and the corresponding values are $\sigma = -3.273 \cdot 10^{-1}$, $\beta_1 = 7.323 \cdot 10^{-1}$, $\beta_2 = -9.20 \cdot 10^{-1}$, $\beta_3 = 3.566 \cdot 10^{-1}$. The constraint parameters at other positions also basically satisfy this formula, but coefficients are different.

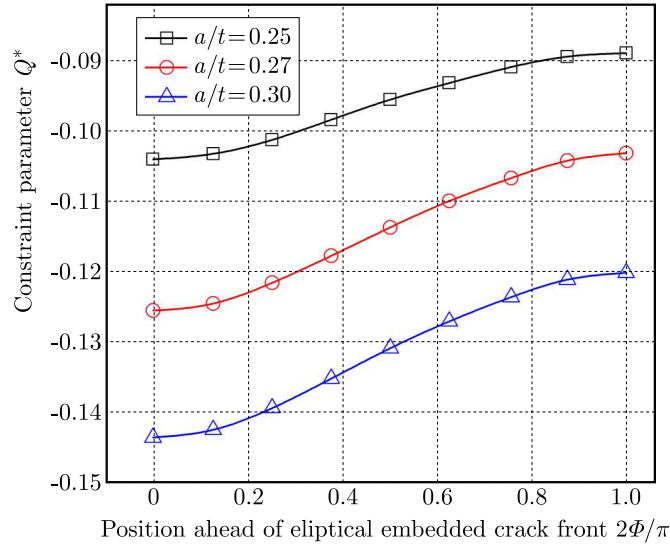


Fig. 6. Distributions of the constraint parameter ahead of the crack front for cracks with various depths with $a/c = 0.7$

Figure 6 compares the distribution of the constraint parameter Q^* varied with the angle position ($0 \leq 2\Phi/\pi \leq 1$) ahead of the elliptical crack front with the crack length ratio $a/c = 0.7$ and depth ratio $a/t = 0.25, 0.30, 0.35, 0.40$. It can be concluded that the variation of crack depth ratio a/t has a negative correlation with the constraint parameter Q^* around the crack front, that is, the larger the crack longitudinal length a is, the smaller the constraint parameter Q^* is. This is due to the fact that with an increase of a , the outline of elliptical crack front is closer to a circle, and the tension stress will be smaller at the endpoint of the crack front. Since the model is only 1/8 part of the plate structure, the critical crack size must meet $a/t < 0.5$ according to the actual value of a and t (that is, the crack length a in the plate thickness direction cannot exceed half of the plate thickness $t/2$). By analyzing each group of data of the constraint parameter with a fixed depth ratio, it can be found that the change of the constraint parameter Q^* varies with the angle $2\Phi/\pi$ showing an upward trend, which is similar with what discussed in Fig. 5. For the elliptical embedded crack with $a/c \leq 1.0$, the maximum value of the constraint parameter Q^* is distributed at the position of $2\Phi/\pi = 1$, and for the elliptical embedded crack with $a/c \geq 1.0$,

the maximum value of the constraint parameter Q^* is distributed at the position of $2\Phi/\pi = 0$. Additionally, with an increase of the crack depth ratio a/t , the constraint parameter at the deepest point of the crack (the endpoint of the long axis of the elliptical crack) is larger, which means that the stress concentration is more serious and the location is more dangerous.

3.2. Results and analysis of creep crack initiation

To study creep damage accumulation along the elliptical embedded crack front and to determine creep crack initiation time, it is necessary to define the critical distance ahead of the crack tip, which will be used in the finite element model to obtain the damage value and creep crack initiation time. The definition of the critical location of creep crack initiation time should follow the detailed principles: (i) firstly to determine the angle $2\Phi/\pi$ ahead of the crack front (that is, the maximum angle position of the constraint parameter obtained from analysis in the previous Section), (ii) then a critical distance away from the crack front also needs to be chosen as the research position of the creep crack initiation process, which is generally selected as the characteristic grain size of P92 heat-resistant steel about $d = 0.05$ mm. The details are depicted by using the example shown in Fig. 7.

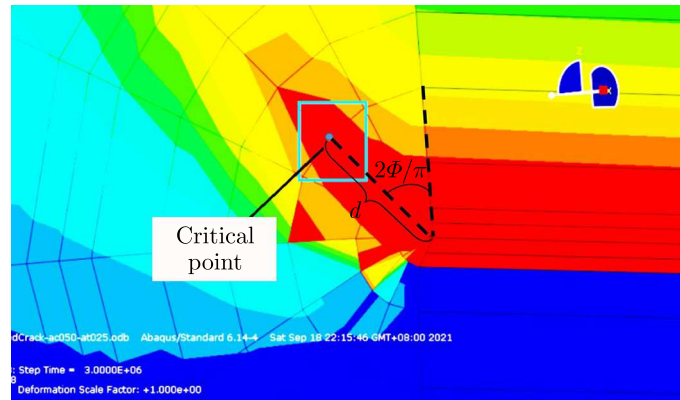


Fig. 7. Definition of the critical position of creep crack initiation time in the FE model

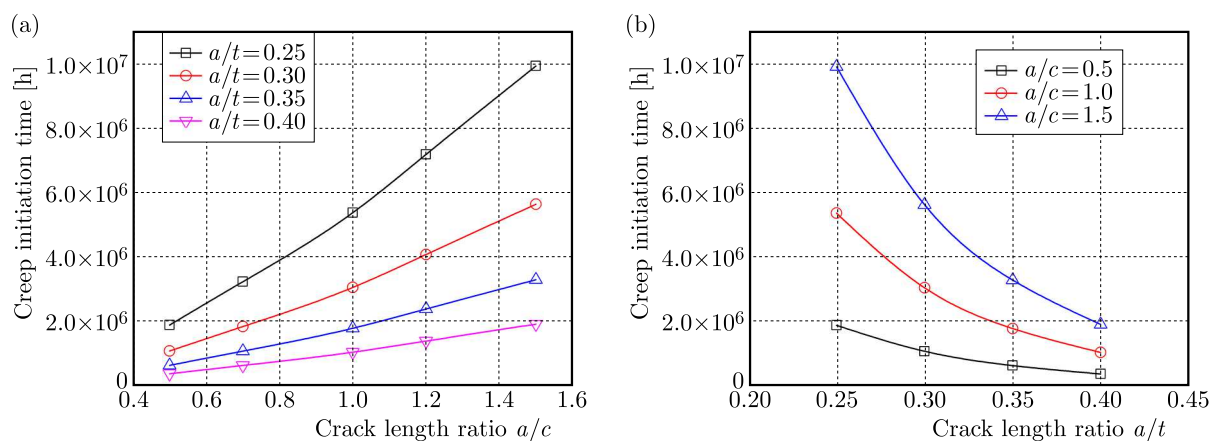


Fig. 8. Variations of the creep crack initiation time with: (a) a/c , (b) a/t

Figure 8a compares the relationship between the crack length ratio a/c and the creep crack initiation time when the crack depth ratio a/t is fixed. The results show that the creep crack initiation time decreases with a decrease of the crack length ratio a/c , which is similar with the change of constraint levels. Figure 8b compares the relationship between the crack depth

ratio a/t and the creep crack initiation time when the crack length ratio a/c is fixed. With an increase of crack depth ratio a/t , the creep crack initiation time is shortened, which also keeps consistent with the change of the constraint level. Therefore, it can be indicated that the longer the crack length and the deeper the crack depth are, the stronger the constraint effect ahead of the crack front is, the faster accumulation of creep damage and creep crack cracking, as well as the shorter the creep crack initiation time, and the more endangered the structure. Note that in this Section, the constant distributed load of 30 MPa is applied for different sizes of embedded cracks.

Meanwhile, it can be found from Fig. 8 that the relationship between the creep crack initiation time t_i and crack depth ratio a/t meets an exponential law. By fitting the data in Fig. 8a, the engineering calculation method between the creep crack initiation time t_i and crack depth ratio a/t under different crack length ratio a/c can be established respectively

$$t_i = \begin{cases} 3E + 7 \exp\left(-11.06\frac{a}{t}\right) & \text{for } \frac{a}{c} = 0.5 \\ 8E + 7 \exp\left(-11.05\frac{a}{t}\right) & \text{for } \frac{a}{c} = 1.0 \\ 2E + 8 \exp\left(-11.05\frac{a}{t}\right) & \text{for } \frac{a}{c} = 1.5 \end{cases} \quad (3.2)$$

It can be found that the above formulas are basically similar, so the engineering calculation method between the creep crack initiation time t_i and crack depth ratio a/t can be summarized by a unified expression

$$t_i = A \exp\left(B\frac{a}{t}\right) \quad (3.3)$$

where the exponent terms of the formula are basically the same $-11.05a/t$, that is, the exponent coefficient $B = -11.05$. The coefficient term A of the formula is related to the crack length ratio a/c . The relationship between A and a/c basically meet an exponential law, and it can be fitted as follows

$$A = 1E + 7 \exp\left(1.8971\frac{a}{c}\right) \quad (3.4)$$

By taking Eq. (3.4) into Eq. (3.3), the relationship between the creep crack initiation time t_i and crack depth ratio a/t as well as crack length ratio a/c can be further written as

$$t_i = \left[1E + 7 \exp\left(1.8971\frac{a}{c}\right)\right] \exp\left(-11.05\frac{a}{t}\right) \quad (3.5)$$

In addition, the variation of creep crack initiation time under different loads is also studied. Taking the model with crack sizes of $a/c = 0.5$, $a/t = 0.3$ as an example, the simulation results of the creep crack initiation time for different loads are shown in Fig. 9. It is obvious that, with an increase of load P , the creep crack initiation time of the plate structure decreases gradually, and it changes linearly in the logarithmic coordinate. Based on the findings, we can draw a conclusion that the load is an important factor which leads to a rapid increase of creep damage and a reduction of creep life of the plate structure containing an elliptical embedded crack.

Moreover, it can be found that the relationship between creep crack initiation time t_i and load P satisfies the exponential relationship, namely, the engineering calculation method for the creep crack initiation time and load can be expressed by the following formula

$$t_i = 1.263E + 9 \exp(-0.23P) \quad (3.6)$$

Since the curves for creep crack initiation time t_i against the load P under different crack sizes are similar and show the exponential law, the relationship between creep the crack initiation

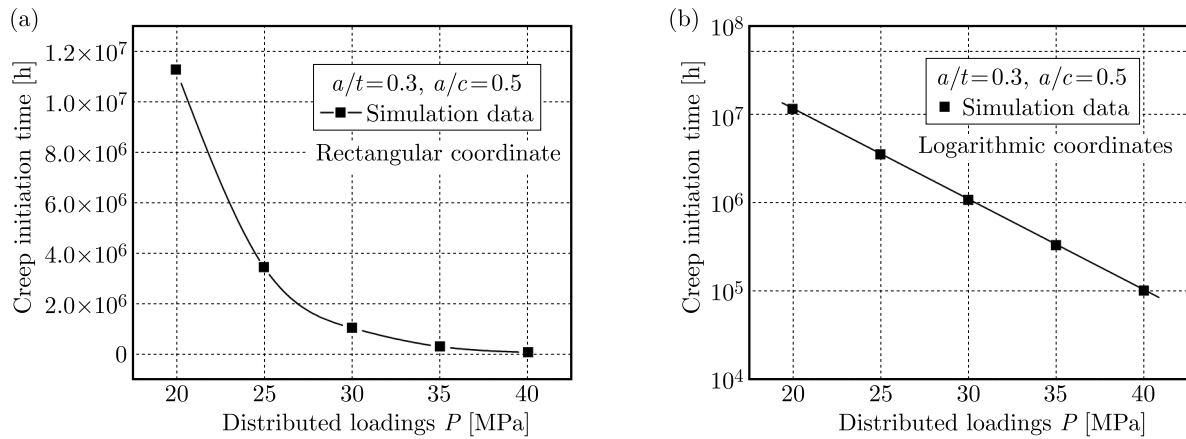


Fig. 9. Variations of the creep crack initiation time under different loadings: (a) in rectangular coordinate, (b) in logarithmic coordinate

time and crack depth ratio a/t as well as crack length ratio a/c and load P can be established by referring to Eq. (3.5) and Eq. (3.6)

$$t_i = 1.124E + 8 \exp\left(0.94855 \frac{a}{c} - 5.525 \frac{a}{t} - 0.115P\right) \quad (3.7)$$

Based on the above engineering prediction formula, the creep crack initiation time of the plate structure containing the elliptical embedded crack with a specified crack size and load can be predicted. In the following study, four groups of non-fitting data of plate structures with embedded cracks are selected for finite element simulation as summarized in Table 3, and the results are compared with the calculation results of the engineering prediction formula, see Fig. 10. It can be found that the engineering predictions for different control groups have better accuracy than the simulation results, and the error can be kept within $\pm 5\%$, which verifies the validity of the engineering prediction formula for the creep crack initiation time.

Table 3. Comparison of creep crack initiation times between FE results and predictions for different conditions

Specimen	Parameter					
	a/t	a/c	P [MPa]	Simulation results [h]	Predictions from equation [h]	Error [%]
1	0.32	0.8	23	$2.997 \cdot 10^6$	$2.911 \cdot 10^6$	-2.8
2	0.38	1.2	38	$5.329 \cdot 10^5$	$5.437 \cdot 10^5$	2.0
3	0.38	0.8	38	$3.795 \cdot 10^5$	$3.721 \cdot 10^5$	-1.9
4	0.32	1.2	23	$4.167 \cdot 10^6$	$4.252 \cdot 10^6$	2.0

4. Conclusion

In this study, a high temperature plate structure containing elliptical embedded cracks is taken as the research object. Based on the creep ductility exhaustion model, the constraint effect and creep crack initiation times are studied by using the three-dimensional (3D) finite element method. The results show that:

- When the crack depth ratio a/t is fixed, with an increase of the crack length ratio a/c , the constraint parameter near the shallowest point of the crack front (about $2\Phi/\pi = 1$) increases continuously. Whether the major axis of an elliptical crack is distributed transversely or

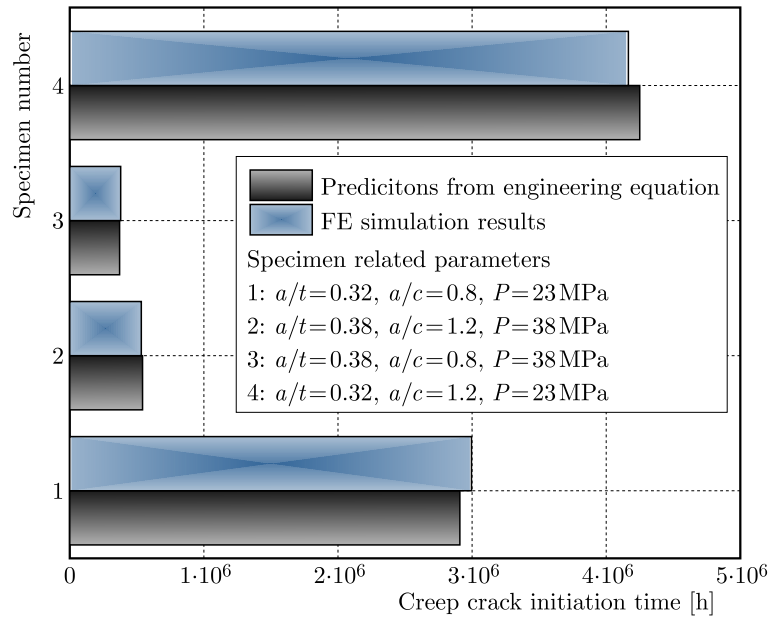


Fig. 10. Comparison of creep crack initiation times between FE results and predictions for different conditions

longitudinally, the maximum constraint level always appear at the endpoint of the actual major axis of the elliptical crack, and the minimum constraint level always appear at the end of the minor axis. When the crack length a/c is fixed, the constraint parameter decreases with an increase of the crack depth ratio a/t , which is due to the fact that the outline of the crack is close to circular.

- With a decrease of the crack length ratio a/c or an increase of the crack depth ratio a/t , the creep crack initiation times decrease significantly. That is, with an increase of the transverse crack length c or the longitudinal crack length a , the creep damage accumulation rate increases, the creep crack initiation time shortens, and the lower the safety of the plate structure is, the easier the creep crack propagation cracking occurs.
- The empirical relationship between the constraint parameter Q^* and embedded crack length and depth is established. The engineering prediction method of creep crack initiation times is also established and validated with the influence of the embedded crack length, crack depth as well as load taken into consideration.

Acknowledgements

The authors would like to acknowledge the support from the Scientific Research Program of Tianjin Education Commission (Grant No. 2021KJ053).

References

1. BUDDEN P.J., AINSWORTH R.A., 1999, The effect of constraint on creep fracture assessments, *International Journal of Fracture*, **97**, 1, 237-247
2. CHEN L., JIANG T., XIE L., 2004, Overview of life prediction methods for turbine blades under creep fatigue interaction, *Aviation Manufacturing Technology*, **12**, 61-64
3. CHEN X., ZHOU G., TU S., 2014, Finite element analysis of creep crack propagation of T-type brazing joints, *Journal of Mechanical Strength*, **5**, 790-796
4. COCKS A.C.F., ASHBY M.F., 1980, Intergranular fracture during power-law creep under multi-axial stresses, *Metal Science*, **14**, 8/9, 395-402

5. DAVIES C.M., 2006, *Crack Initiation and Growth at Elevated Temperatures in Engineering Steels*, Department of Mechanical Engineering, Imperial College London, 1-200
6. DAVIES C.M., O'DOWD N.P., NIKBIN K.M., WEBSTER G.A., 2007, An analytical and computational study of crack initiation under transient creep conditions, *International Journal of Solids and Structures*, **44**, 1823-1843
7. HOLDSWORTH S.R., 1992, Initiation and early growth of creep cracks from pre-existing defects, *Material High Temperature*, **10**, 127-137
8. HOSSEINI E., HOLDSWORTH S., MAZZA E., 2013, Stress regime-dependent creep constitutive model considerations in finite element continuum damage mechanics, *International Journal of Damage Mechanics*, **22**, 8, 1186-1205
9. LIU Y., MURAKAMI S., 1998, Damage localization of conventional creep damage models and proposition of a new model for creep damage analysis, *JSME International Journal Series A*, **41**, 1, 57-65
10. MAO X., LIU Z., YANG K., *et al.*, 2004, Creep damage calculation model based on time-harden theory, *Journal of Mechanical Strength*, **26**, 1, 105-108
11. MURAKAMI S., KAWAI M., RONG H., 1988, Finite element analysis of creep crack growth by a local approach, *International Journal of Mechanical Sciences*, **30**, 7, 491-502
12. RABOTNOV Y.N., LECKIE F.A., PRAGER W., 1970, Creep problems in structural members, *Journal of Applied Mechanics*, **37**, 1, 249
13. RIEDEL H., RICE J.R., 1980, Tensile cracks in creeping solids, *ASTM STP 700, American Society for Testing and Materials*, **1**, 112-130
14. SHIH C.F., GERMAN M.D., 1981, Requirements for a one parameter characterization of crack tip fields by the HRR singularity, *International Journal of Fracture*, **17**, 27-43
15. WEN J.F., TU S.T., 2014, A multiaxial creep-damage model for creep crack growth considering cavity growth and microcrack interaction, *Engineering Fracture Mechanics*, **123**, 197-210
16. WU D.Q., JING H.Y., XU L.Y., 2020, Engineering application of enhanced C^* - Q^* two parameter approaches for predicting creep crack initiation times, *European Journal of Mechanics - A/Solids*, **82**, 104013
17. XU L.Y., ZHANG X.F., ZHAO L., HAN Y., JING H., 2016, Quantifying the creep crack-tip constraint effects using a load-independent constraint parameter Q^* , *International Journal of Mechanical Sciences*, **119**, 320-332
18. YAMAMOTO M., MIURA N., OGATA T.K., 2010, Applicability of C^* parameter in assessing Type IV creep cracking in Mod. 9Cr-1Mo steel welded joint, *Engineering Fracture Mechanics*, **77**, 15, 3022-3034
19. YATOMI M., BETTINSON A.D., O'DOWD N.P., NIKBIN K.M., 2004, Modelling of damage development and failure in notched-bar multiaxial creep tests, *Fatigue and Fracture of Engineering Materials and Structures*, **27**, 4, 283-295
20. YOU Y., LING X., TU S., 2004, Finite element analysis of creep damage of small punch test specimen at elevated temperature, *Journal of Mechanical Strength*, **26**, 2, 183-187
21. ZHAO L., JING H., XU L., HAN Y., XIU J., 2012, Analysis of creep crack growth behavior of P92 steel welded joint by experiment and numerical simulation, *Materials Science and Engineering A*, **558**, 119-128